



Study on the relationship between the water cutting rate and the remaining oil saturation of the reservoir by using the index percolating saturation formula with variable coefficients

Meiling Zhang¹ · Jiayi Fan¹ · Yongchao Zhang¹ · Yinxin Liu¹

Received: 22 April 2020 / Accepted: 30 July 2020 / Published online: 13 August 2020
© The Author(s) 2020

Abstract

The water cutting rate is recorded dynamically during the production process of a well. If the remaining oil saturation of the reservoir can be deduced based on the water cutting rate, it will give guidance to improve the reservoir recovery and can save expensive drilling costs. In the oil–water two-phase seepage experiment on core samples, the oil and water relative permeability reflects the relationship between the water cutting rate and water saturation, that is, percolating saturation formula. The relative permeability test data of 17 rock samples from six seal coring wells in Daqing Changyuan were used to optimize and construct the coefficients of the index percolating saturation formula that vary with the pore structure parameters of reservoirs, to form an index percolating saturation formula with variable coefficients that is more consistent with the regional geological characteristics of the reservoir. Based on this, the formula of water saturation calculated by the water cutting rate is deduced. And the high-precision formula for calculating the irreducible water saturation and residual oil saturation by effective porosity, absolute permeability, and shale content is given. The derivative formula of water saturation on the water cutting rate was established, and the parameters of 17 rock samples were calculated. It was found that the variation velocity of water saturation of each sample with the water cutting rate presented a “U” shape, which was consistent with the actual characteristics that the variation velocity of the water saturation in the early, middle, and late stages of oilfield development first decreased, then stabilized, and finally increased rapidly. The research results were applied to the prediction of remaining oil saturation in the research area, and the water saturation about six producing wells was calculated by using their present water cutting rates, and the remaining oil distribution profile was predicted effectively. The analysis of four layers of two newly drilled infill wells and reasonable oil recovery suggestions were given to achieve good results.

Keywords Relative permeability · Variable coefficient · Index percolating saturation formula · Water cutting rate · Remaining oil saturation · Daqing Changyuan

Introduction

Some quantitative evaluation methods of remaining oil saturation, such as drilling core method, logging method, and reservoir dynamic production simulation method, have their limitations. It has become a practical and effective method to comprehensively determine the remaining oil saturation of oil reservoirs from the aspects of geology, logging, production dynamics, etc. (Elkins and Poppe 1973; Li and Chen

2001); especially, it is more meaningful to study the distribution characteristics of remaining oil by using the data of seal coring wells at present (Hirasaki 1996). Based on the numerical simulation of experimental data, the effects of relative permeability, capillary pressure, and reservoir parameters on the recovery rate of the water-driven reservoir are deduced (Alfarge et al. 2017). Li et al. (2016) reasonably deduced the water flooding status of underground strata based on seal coring samples. Andersen et al. (2017) constructed a theoretical relationship of the water saturation equation about porosity, relative permeability, and capillary pressure from the perspective of core experiment; Zahoor (2015) used relative permeability data to study the saturation state of the displacement fluid in porous media.

✉ Meiling Zhang
zhangmeiling8@163.com

¹ School of Earth Science, Northeast Petroleum University, Daqing 163318, China

The porosity (ϕ), absolute permeability (k) (according to the convention, the word permeability in the text refers to absolute permeability except for the relative permeability), and shale content of core samples are routine measurement items of reservoir physical property experiments. They have been perfected from measuring instruments to measuring techniques (Shen et al. 1995). As the basic data of scientific research, core samples are all to measure porosity, air permeability, and shale content. When conducting immiscible fluid displacement experiments in porous media, Dullien et al. (1972) found that the fluid flow state in pores and the capillary pressure suffered by the fluid were firmly related to the pore structure. Experiments show that the pore structure parameter (R_c) has a good correlation with $\sqrt{k/\phi}$, i.e., the root mean square of the ratio of permeability (k) and porosity (ϕ) (Pittman 1992; Lala and El-Sayed 2015). At present, this parameter has been used to establish the calculation formula of the oil saturation (S_o) suitable for low porosity–permeability reservoirs and obtained excellent results in the evaluation of the distribution of oil and water in complex reservoirs (Zhang et al. 2013).

The water cutting rate of the dynamic reservoir production reflects the characteristics of water flooding remaining oil in actual oil engineering (Renard et al. 1998). Hu et al. (2005) established the linear equation between water cutting rate and water saturation by taking the tertiary oil layers of Jiyang depression as the research object and pointed out that the coefficients in the formula are closely related to the porosity of the rock.

The experimental relative permeability is the link that establishes the relationship between water flooding characteristics and remaining oil saturation. This procedure is called percolating saturation formula. Zhang et al. (2018) studied the relationship between water cutting rate content and relative permeability measured from the experiment, which was used to study the variation trend of water cutting rate in the actual production, and the relatively suitable results were obtained. Feng et al. (2017) established a water-driven state prediction model from the linear correlation between relative permeability and water saturation. Xu et al. (2014) used the regression analysis method to fit the relative permeability curve and established the calculation formula of oil–water relative permeability and water saturation, to predict the remaining oil reserves. At present, the percolating saturation formula commonly used includes the exponential method and indexing method (Cobb and Marek 1997). The exponential method is simple and does not take the irreducible water and residual oil saturation into account, and the form is commonly used to analyze the relationship between oil displacement efficiency and water cutting rate (Gong et al. 2018). The formula of index percolating saturation formula contains two parameters of bound water saturation and residual oil saturation, which can reflect

the prediction of remaining oil saturation more practically. Yang (1998) used index percolating saturation formula with fixed coefficients (c , n) to establish the compute method of remaining oil saturation in the west part of the seventh block of Gudong oilfield.

The percolation saturation relationship is from the core experiment, which combines the water production rate and water saturation, and reflects the reasonable formula of fluid seepage. Based on the experimental relative permeability in the coring wells, we were combining the index percolating saturation formula and the water-driving seepage formula and got the formula for calculating the remaining oil saturation by water cutting rate. In this paper, we found the coefficients of the index percolating saturation formula are related to the porosity and permeability of rock samples, so we optimally established the variable coefficients' formula. The introduction of the variable coefficients index method is innovative because it can effectively investigate the variation trend of remaining oil saturation in reservoirs with different porosity and permeability, even though under the condition that the variation of water cutting rate is the same. Moreover, it reflects the actual situation that the flowing fluid in the rock layer is subject to porosity and permeability conditions (An et al. 2016), and the calculation results are more reliable with strong practicality. The realization process of this method is reasonable that can be extended to other oilfields that have been developed for many years to predict the remaining oil saturation or determine the position of drilling new wells.

Methodology

Because of the complexity of the pore structure, water cannot thoroughly wash away the oil where it sweeps. From the injection side to the production side, the distribution of water saturation of a sand layer is discontinuous unless the injection water arrived at the production well, and the oil–water front is formed at the abrupt change of water saturation. The water saturation of the area between the oil–water front and the injection side increases gradually, where the oil and water typically flow in a two-phase way. Between the oil–water front and the oil-producing end, the pure oil flow zone occurs where the water is bound, and oil can flow freely. The oil–water front moves in the direction of the injection toward production over time, that is, the two-phase flow zone keeps expanding, and the pure oil zone keeps shrinking. When injection water appears at the producing end, only the two-phase flow zone remains in the reservoir (Rathmell et al. 1973). Based on Buckley–Levrett's one-dimensional two-phase leading-edge displacement theory, we proposed an unsteady oil–water relative permeability measurement method for displacement experiment data (Welge et al. 1962). According to the simulation

conditions, The experiment with the constant pressure difference or constant velocity is carried out on the rock sample, then the outputs (q_o , q_w) of oil and water at the rock sample outlet are recorded. While the pressure difference across the core changes with time, we can use the Darcy formula to calculate oil–water relative permeability (k_{ro} , k_{rw}). Meanwhile, we use the weighing method or the material balance method to calculate the corresponding oil–water saturation value (S_o , S_w) of the rock samples. During the experiment, the ratio of oil to water was changed, the proportion of oil gradually decreased, the proportion of water gradually increased, and the distribution of water and oil saturation in porous media was a function of distance and time.

In this way, we obtained a series of oil and water relative permeability values at different water saturation values, and the relationship curve between the oil and water relative permeability and water saturation of rock samples can be drawn (Xie et al. 2003).

The oil–water relative permeability displacement experiment can also give the measured values of bound water saturation and residual oil saturation. In the process of displacing water with oil rapidly, as the oil saturation of the pore space gradually increases, the oil first occupies the part of the pore space where the fluid flow resistance is the smallest, the relative permeability k_{rw} gradually approaches 0, the water yield $q_w \rightarrow 0$, water cutting rate $f_w \rightarrow 0$, and water is mainly distributed in tiny capillaries where the fluid is not natural to flow or adsorbed on the surface of the rock particles, which is the bound water saturation S_{wi} . In the process of displacing oil with water, the oil relative permeability k_{ro} gradually approaches 0, oil yield $q_o \rightarrow 0$, the water cutting rate $f_w \rightarrow 1$, while the oil saturation is the residual oil saturation S_{or} .

Suppose that the cross section of the horizontal stratum remains constant, one side injected water and the other side produces oil. k is the permeability (i.e., absolute permeability) of the horizontal formation, mD (i.e., $10^{-3} \mu\text{m}^2$), and μ_o and μ_w are the viscosity of oil and water, respectively, mPa s. The pressure gradient at some time point on a cross section is $\frac{\partial p}{\partial x}$, and the seepage velocity of water at the interface multiplied by the cross-sectional area (A') of the formation should be equal to the flow water yield, q_w . According to Darcy's law,

$$q_w = k \cdot A' \cdot \frac{k_{rw}}{\mu_w} \cdot \frac{\partial p}{\partial x} \quad (1)$$

Capillary pressure is not considered in the same section. The pressure gradient of water and oil is the same. The flow of oil yield q_o is equal to:

$$q_o = k \cdot A' \cdot \frac{k_{ro}}{\mu_o} \cdot \frac{\partial p}{\partial x} \quad (2)$$

From Eqs. (1) and (2), we obtained the water cutting rate on the cross section:

$$f_w = \frac{q_w}{q_w + q_o} = \frac{1}{1 + \frac{\mu_w}{\mu_o} \cdot \frac{k_{ro}}{k_{rw}}} \quad (3)$$

Equation (3) indicates that the relative permeability of oil and water determines whether the reservoir produces oil, water, or both. Moreover, the change of relative permeability of oil phase and water phase with water saturation can be expressed by index percolating saturation formula (Yu 1982):

$$\frac{k_{ro}}{k_{rw}} = c \left(\frac{S_w - S_{wi}}{1 - S_{or} - S_w} \right)^{-n} \quad (4)$$

where S_w —water saturation, decimal; S_{or} —residual oil saturation after water flooding, decimal; S_{wi} —formation bound water saturation, decimal.

Some studies show the relative permeability is related to many factors such as rock pore structure, rock wettability, and oil–water viscosity ratio (Burdine 1953; Singh et al. 2019; Crotti and Cobenas 2001), so the coefficients c and n in formula (4) are naturally influenced by oil–water viscosity ratio and rock pore structure. Formula (4) indicates that the oil–water relative permeability and water saturation of a core sample have various corresponding relationships. Through Eqs. (3) and (4), the relationship between f_w , S_w , S_{wi} , and S_{or} can be deduced, see (5):

$$S_w = \frac{\left(\frac{cf_w}{1-f_w} \cdot \frac{\mu_w}{\mu_o} \right)^{\frac{1}{n}} (1 - S_{or}) + S_{wi}}{1 + \left(\frac{cf_w}{1-f_w} \cdot \frac{\mu_w}{\mu_o} \right)^{\frac{1}{n}}} \quad (5)$$

$$S_o = 1 - S_w \quad (6)$$

According to formulas (5) and (6), when the water productivity at the outlet of a rock layer is known, the water saturation S_w and remaining oil saturation S_o of a rock can be calculated.

Determination of coefficients c and n

According to the standard of relative permeability in the oil and gas industry and related experiment implementation methods (Jones and Roszelle 1978), we selected 17 rock samples from six seal coring wells in Daqing Changyuan oilfield for relative permeability test in this paper. The porosity of these cores ranges from 24.5 to 32.2%, and the permeability ranges from 14.6 to 1632.7 mD. They can capture the porosity and permeability characteristics of Daqing Changyuan oilfield (Hou et al. 2009). Table 1 shows the test parameters. The simulated oil viscosity, density, and the injection

Table 1 Experimental conditions for oil–water relative permeability test

Sample type	Simulated oil viscosity	Simulated oil density	Temperature	Injected water viscosity	Injected water density
Sandstone	7.96 (mPa S)	0.837 (g/cm ³)	45 (°C)	0.621 (mPa S)	0.995 (g/cm ³)

viscosity and density are consistent with the produced oil and injected water in the block where the core wells located.

According to formula (4), the coefficients c and n are influenced by the rock pore structure, wettability, and oil–water viscosity ratio. Because the samples come from the same oil group in a development block, they have almost the same wettability and oil–water viscosity ratio. In the actual calculation, it can be determined uniformly according to the development time stage and the block position. We focused on establishing the relationship between coefficients c and n and the rock pore structure parameter R_c :

$$R_c = \sqrt{k/\varphi} \quad (7)$$

Take the natural logarithm of both sides of Eq. (4) to obtain Eq. (7):

$$\ln\left(\frac{k_{ro}}{k_{rw}}\right) \ln(c) - n \ln\left(\frac{S_w - S_{wi}}{1 - S_{or} - S_w}\right) \quad (8)$$

Let

$$x = \ln\left(\frac{S_w - S_{wi}}{1 - S_{or} - S_w}\right) \quad (9)$$

$$y = \ln\left(\frac{k_{ro}}{k_{rw}}\right) \quad (10)$$

x and y of each sample are calculated, respectively, according to Eqs. (9) and (10). From Eq. (8), we can fit a linear regression line about y with respect to x of each sample. The slope of the line is $(-n)$, and the intercept is $\ln(c)$. Figure 1 shows y and x cross-plot of 17 rock samples. For clearly showing, we put the samples into four sub-figures. And Table 2 shows the formula of the relationships between $\ln\left(\frac{S_w - S_{wi}}{1 - S_{or} - S_w}\right)$ and $\ln\left(\frac{k_{ro}}{k_{rw}}\right)$. Table 2 also gives the correlation coefficients (R^2), standard deviations of x and y of each sample, and the root mean square error (RMSE). From the data, we can find good fitness of x and y for each sample.

Table 3 shows the data of porosity (φ), permeability (k), bound water saturation (S_{wi}), residual oil saturation (S_{or}), and shale content (V_{sh}) of 17 samples, and the last two columns in Table 3 are $\ln(c)$ and n . Figure 1 shows each sample has a good correlation between y and x , and the range of n between different samples is small. In these samples, No. 363 has the lowest value ($n = 1.461$), and No. 520 has the

highest value ($n = 1.788$); but $\ln(c)$ varies widely: change from -0.204 of sample No. 1107 to 1.701 of sample No. 733, that is, the varying range of c value is 0.815 – 5.480 .

There is a good positive correlation between the size of the pore throat and R_c ($\sqrt{k/\varphi}$) value (Ma and Morrow 1996). Formula (7) is used to calculate the R_c values of 17 samples, as shown in column 7 in Table 3. Analyze the relationship between φ , k , R_c values with n and $\ln(c)$ of each sample: Sample No. 363 has the minimum value of n , and its values of φ , k , and R_c are 30.6%, 1632.7 mD, and 7.306; sample No. 520 has the maximum value of n , and its φ , k , and R_c values are 24.6%, 35.6 mD, and 1.203; sample No. 1107 has the minimum value of $\ln(c)$, and its values of φ , k , and R_c are 30.6%, 1632.7 mD and 7.306; sample No. 733 has the maximum value of $\ln(c)$, and its values of φ , k , and R_c are 30.6%, 1632.7 mD, and 7.306. These data further illustrate the point above that n and $\ln(c)$ are affected by the porosity and permeability of a rock layer. Figure 2 shows the relationship between R_c and $\ln(c)$ and reflects the positive correlation between the two; the correlation equation is shown in Eq. (11), correlation coefficient (R^2) is 0.801, and the root mean square error (RMSE) is 0.132. It shows that the larger the pore throat, the larger the coefficient c ; Fig. 3 shows the relationship between R_c and n , R_c is negatively correlated with n , and the relation is shown in Eq. (12), correlation coefficient (R^2) is 0.859, and the root mean square error (RMSE) is 0.311:

$$\ln(c) = 0.2595R_c - 0.2335 \quad (11)$$

$$n = -0.044R_c + 1.8221 \quad (12)$$

Determination of bound water saturation (S_{wi}) and residual oil saturation (S_{or})

The bound water and residual oil remain in the micropores of sandstone or are adsorbed on the surface of the particles with large pore by the molecular surface force and cannot flow freely. The good residual oil saturation and bound water saturation can be deduced by the core analysis data in the water flooding area (Abrams 1975).

The study area has shaly sandstone sedimentary strata, the more micro-channels in the sandstone strata, the lower permeability, and the more residual stagnant water. The more the

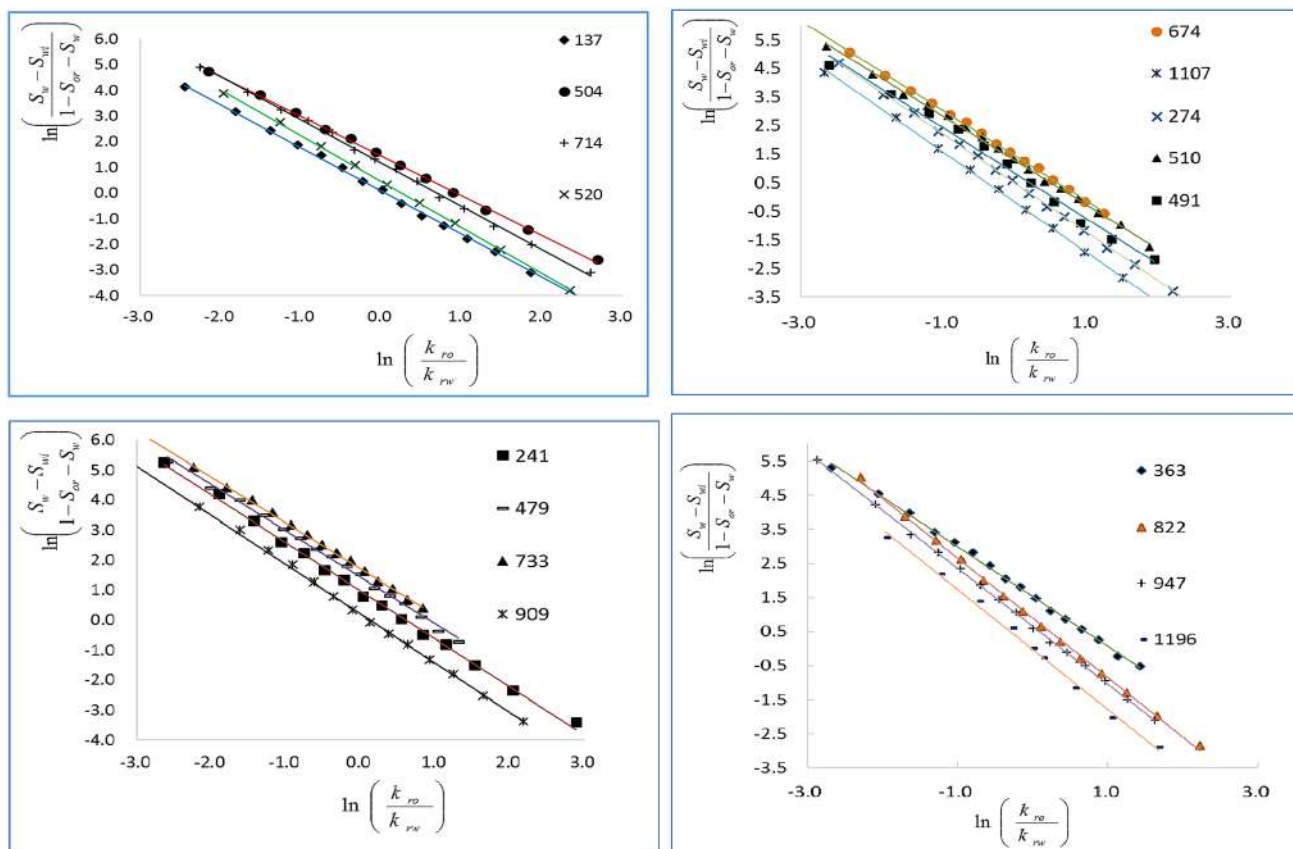


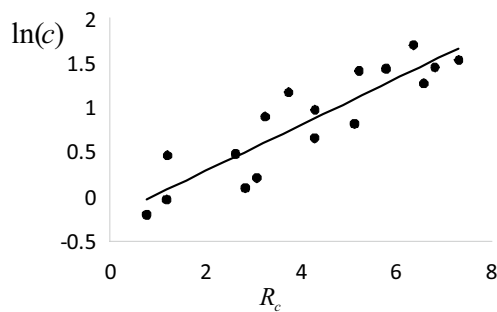
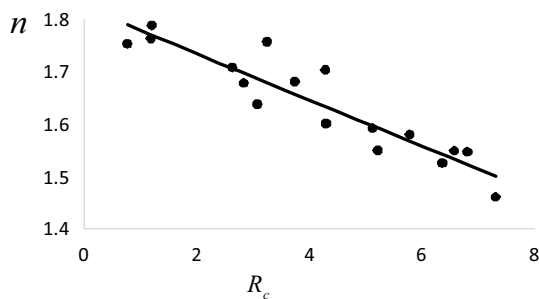
Fig. 1 Cross-plots of different samples between $\ln\left(\frac{S_w - S_{wi}}{1 - S_{or} - S_w}\right)$ and $\ln\left(\frac{k_{ro}}{k_{rw}}\right)$. (Numbers in the legend are the sample numbers. The lines in the sub-figures are linear regression trend lines)

Table 2 The formula of the relationships for 17 samples and the relative analysis data on fitness

Sample number	Formula of the relationships	Correlation coefficients (R^2)	SD (x, y)	Root mean square error (RMSE)
363	$y = -1.4607x + 1.5314$	0.9983	1.1362, 1.6597	0.0694
504	$y = -1.5466x + 1.4511$	0.9991	1.3496, 2.0874	0.0619
510	$y = -1.5487x + 1.2674$	0.9985	1.2317, 1.9076	0.0740
733	$y = -1.5261x + 1.7011$	0.9990	1.0558, 1.6113	0.0505
674	$y = -1.5797x + 1.4320$	0.9994	1.1908, 1.8811	0.0469
479	$y = -1.5500x + 1.4087$	0.9969	1.0884, 1.6869	0.0979
491	$y = -1.5924x + 0.8174$	0.9904	1.2987, 2.0680	0.2033
241	$y = -1.6010x + 0.9713$	0.9980	1.4566, 2.3320	0.1048
947	$y = -1.7025x + 0.6560$	0.9996	1.2312, 2.0962	0.0420
714	$y = -1.6810x + 1.1694$	0.9986	1.3300, 2.2358	0.0843
822	$y = -1.7572x + 0.8964$	0.9991	1.2502, 2.1969	0.0673
909	$y = -1.6381x + 0.2091$	0.9987	1.4086, 2.3074	0.0845
137	$y = -1.6781x + 0.0951$	0.9988	1.3430, 2.2535	0.0782
274	$y = -1.7077x + 0.4779$	0.9997	1.4605, 2.4942	0.0423
520	$y = -1.7878x + 0.4606$	0.9997	1.2819, 2.2918	0.0412
1196	$y = -1.7632x - 0.0346$	0.9959	1.1227, 1.9801	0.1263
1107	$y = -1.7532x - 0.2041$	0.9994	1.4277, 2.5031	0.0611

Table 3 Experimental parameters of different samples and the values of $\ln(c)$ and n

Sample number	Porosity (%)	Permeability (mD)	Bound water saturation (%)	Residual oil saturation (%)	Shale content (%)	R_c	n	$\ln(c)$
363	30.6	1632.7	20.8	20.7	9.0	7.306	1.461	1.531
504	29.2	1352.3	26.5	18.1	7.4	6.805	1.547	1.451
510	31.3	1352.3	18.9	18.7	8.0	6.573	1.549	1.267
733	32.2	1301.9	19.1	19.1	9.4	6.358	1.526	1.701
674	31.1	1040.5	24.5	20.9	11.0	5.784	1.580	1.432
479	29.0	789.2	26.4	21.4	8.5	5.217	1.550	1.409
491	28.0	734.1	35.4	25.6	15.0	5.121	1.592	0.817
241	24.7	455.5	34.9	23.4	12.3	4.294	1.601	0.971
947	29.5	541.6	35.1	20.1	19.8	4.285	1.703	0.656
714	27.2	380.0	36.3	24.8	22.9	3.741	1.681	1.169
822	27.8	293.5	36.3	23.6	13.1	3.249	1.757	0.896
909	27.9	263.8	40.8	24.4	34.6	3.075	1.638	0.209
137	26.3	211.1	41.5	22.5	24.3	2.833	1.678	0.095
274	27.1	187.3	39.2	26.3	31.2	2.629	1.708	0.478
520	24.6	35.6	47.4	27.3	38.7	1.203	1.788	0.461
1196	24.5	34.4	42.0	33.6	26.5	1.185	1.763	-0.035
1107	24.8	14.6	45.8	27.7	28.4	0.767	1.753	-0.204

**Fig. 2** Correlation diagram between R_c and $\ln(c)$ of 17 samples**Fig. 3** Correlation diagram between R_c and n of 17 samples

shaly particles in sandstone, the higher the shale content, and the higher the adsorbed water content on the surface of shaliness particles. Figure 4a, b shows the relationship between shale content (V_{sh}), permeability (k), and bound water saturation (S_{wi}), respectively. The formula of bound water saturation with V_{sh} and the logarithm term (base 10) of k was established, see Eq. (13). The correlation coefficient (R^2) is 0.952, and the root mean square error (RMSE) is 0.103:

$$S_{wi} = 0.4364 - 0.0799 \log(k) + 0.4156V_{sh} \quad (13)$$

Residual oil saturation is related to the oil viscosity, porosity, and permeability of the rock strata. Core experiments show that with the same viscosity, the higher the porosity and permeability, the lower the residual oil saturation (Xie et al. 2017). It is found that the porosity and permeability distribution of core samples can affect the sweep rate of oil–water seepage. Figure 5a, b shows the relationship between porosity (ϕ) and the logarithm term (base 10) of permeability ($\ln k$) with residual oil saturation (S_{or}), respectively. Furthermore, use them to establish the formula of residual oil saturation, see Eq. (14). The correlation coefficient (R^2) is 0.861, and the root mean square error (RMSE) is 0.293:

$$S_{or} = 0.447 - 0.386\phi - 0.0426 \log(k) \quad (14)$$

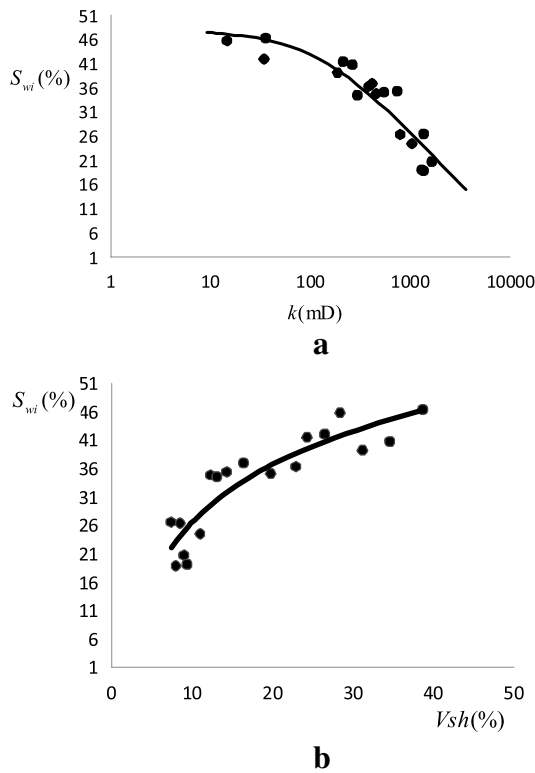


Fig. 4 **a** Correlation diagram of permeability (k) and bound water saturation (S_{wi}), **b** correlation diagram of shale content (V_{sh}) and bound water saturation (S_{wi})

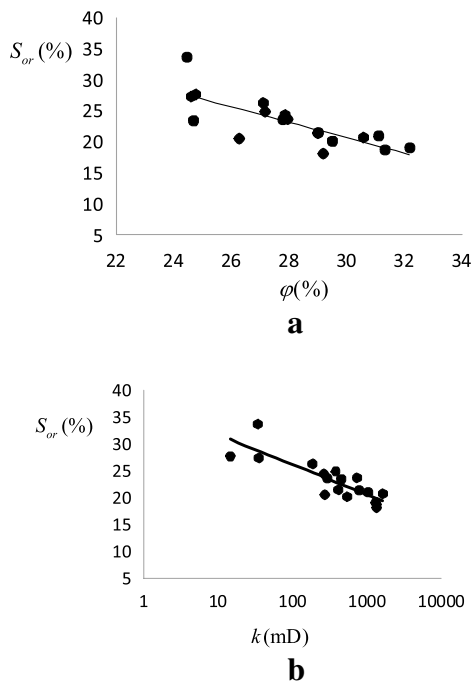


Fig. 5 **a** Correlation diagram of porosity (ϕ) and permeability (k), **b** correlation diagram of porosity (ϕ) and residual oil saturation (S_{or})

Discuss the changing trend of S_w with f_w

After determining the n and c values of each sample, formula (5) can be used to investigate the changing relationship between the water cutting rate f_w and the remaining oil saturation ($1 - S_w$) at the oilfield development stage. For Eq. (5), the derivative of S_w with respect to f_w is calculated as $S'_w(f_w)$, and we get Eq. (15):

$$S'_w(f_w) = \frac{(1 - S_{or} - S_{wi}) \left(\xi^{\frac{1}{n}}\right)'}{\left(1 + \xi^{\frac{1}{n}}\right)^2} \tag{15}$$

where $\xi = \frac{cf_w}{1-f_w} \cdot \frac{\mu_w}{\mu_o}$, $\left(\xi^{\frac{1}{n}}\right)' = \frac{1}{n} \xi^{\frac{1}{n}-1} \xi'(f_w)$, $\xi'(f_w) = \frac{\mu_w}{\mu_o} \frac{c}{(1-f_w)^2}$. $S'_w(f_w)$ is defined as the change rate of water saturation with f_w , S_{or} , S_{wi} , c , and n of the 17 samples in Table 3, and the μ_o , μ_w values in Table 1 are substituted into Eq. (15). For f_w to go from 1 to 99%, with a span of 5%, the change of $S'_w(f_w)$ can be calculated. We tried to use the computer way to divide these samples into clusters (Haralick and Shanmugam 2007) and found that dividing them into three types according to the values of R_c and V_{sh} has the most apparent degree of data separation. This also coincides with the view that porosity, permeability, and mud content are the main factors of stratification (Lu et al. 1995). In the first type group, $R_c \geq 5.0$ and $V_{sh} < 10\%$, which means the samples of this type own the best porosity and permeability characteristic with little shaleness. In the second type group, $R_c \geq 3.0$ and $10\% \leq V_{sh} < 25\%$, which means the samples are shale-bearing sandstone with better porosity and permeability characteristic. In the third group, $R_c < 3.0$ or $V_{sh} \geq 25\%$, which means the samples own the common porosity and permeability characteristic or contain more shaleness. It can be seen that the changing trend of $S'_w(f_w)$ with f_w of samples in the same type is similar in Fig. 6a–c. Figure 6d shows the average trend of each type.

Figure 6 shows that as the water cutting rate f_w increases, when the water cutting rate f_w is less than 20%, the change rate of water saturation $S'_w(f_w)$ shows a decreasing trend. When the water cutting rate f_w is between 20 and 80%, the change rate $S'_w(f_w)$ is about a constant. When the water cutting rate f_w reaches more than 80%, the change rate of water saturation $S'_w(f_w)$ presents a rapidly rising trend. Because the physical properties of samples are different, their changing states are also different. By analyzing Fig. 6d, we obtained the following laws:

1. Samples in the first type group have fine porosity and permeability conditions and low shale content. When the water cutting rate f_w is 1%, the change rate of water saturation $S'_w(f_w)$ is 0.831; with the increase in the water cutting rate, the change rate of water saturation $S'_w(f_w)$

decreases. When the water cutting rate f_w reaches 20%, the change rate of water saturation $S'_w(f_w)$ is 0.305. When the water cutting rate f_w is between 20% and 80%, the change rate of water saturation $S'_w(f_w)$ is flat, and the mean value is 0.331. When the water cutting rate f_w is 80%, the change rate of water saturation $S'_w(f_w)$ reaches 0.546, and then, the change rate of water saturation $S'_w(f_w)$ increased rapidly. When the water cutting rate f_w reaches 99%, the change rate of water saturation $S'_w(f_w)$ is up to 2.972.

2. Samples in the second type group have medium porosity and permeability conditions and medium shaleness. When the water cutting rate f_w is 1%, the change rate of water saturation $S'_w(f_w)$ is 0.557; with the increase in water cutting rate, the change rate of water saturation decreases. When the water cutting rate f_w reaches 20%, the change rate of water saturation $S'_w(f_w)$ is 0.183. When the cutting rate f_w is between 20 and 80%, the change rate of water saturation $S'_w(f_w)$ is flat, and the mean value is 0.211. When the cutting rate f_w is 80%, the change rate of water saturation $S'_w(f_w)$ reaches 0.382, and then,

the change rate of water saturation $S'_w(f_w)$ increased rapidly. When the cutting rate f_w reaches 99%, the change rate of water saturation $S'_w(f_w)$ is up to 3.09.

3. Samples in the third type group have poor pore-permeability conditions and high shale content. When the water cutting rate f_w is 1%, the change rate of water saturation $S'_w(f_w)$ is 0.298; with the increase in water cutting rate f_w , the change rate of water saturation $S'_w(f_w)$ decreases. When the water cutting rate f_w reaches 20%, the change rate of water saturation $S'_w(f_w)$ is 0.100. When the water cutting rate f_w is between 20% and 80%, the change rate of water saturation $S'_w(f_w)$ is flat, and the mean value is 0.125. When the water cutting rate f_w is 80%, the change rate of water saturation $S'_w(f_w)$ reaches 0.254, and then, the change rate of water saturation $S'_w(f_w)$ increased rapidly. When the water cutting rate f_w reaches 99%, the change rate of water saturation $S'_w(f_w)$ is up to 3.01.
4. To summarize the change rate of water saturation $S'_w(f_w)$ with water cutting rate of three types of samples: The condition of porosity and permeability varies from good to bad, and the change rate of water saturation varies from high to low. It indicates that the remaining oil in reservoirs with good porosity and permeability conditions can be reduced quickly. This is consistent with the fact that in actual oilfield exploitation, the injected water

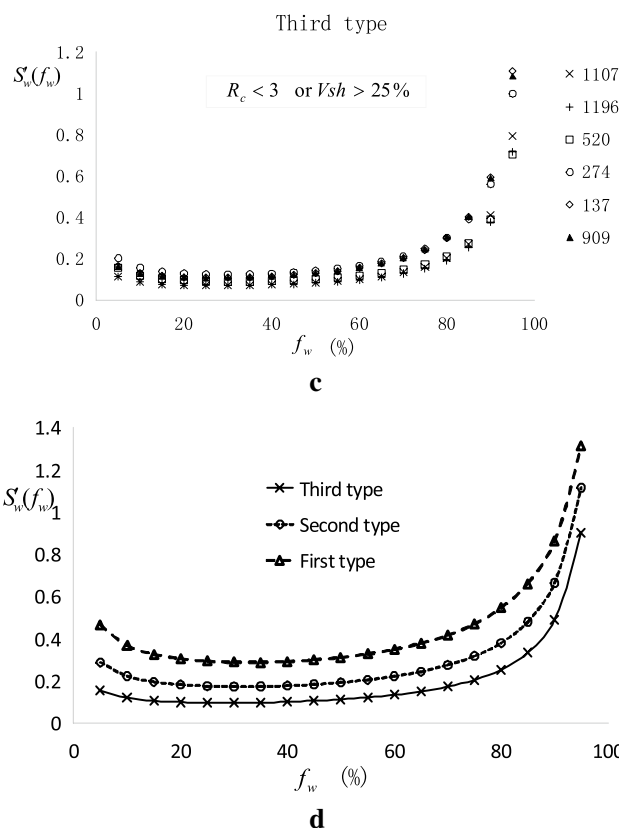
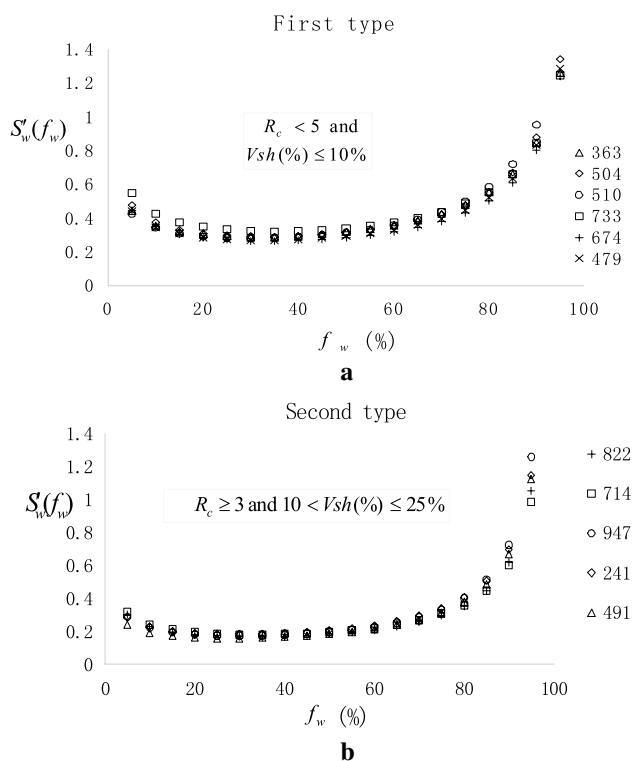


Fig. 6 a The correlation diagram between the water cutting rate and change rate of water saturation of samples in the first type group, **b** the correlation diagram between moisture content and change rate of water saturation of samples in the second type group, **c** the correlation diagram between moisture content and change rate of water saturation of samples in the third type group, **d** correlation diagram between the average water cutting rate and the average change rate of water saturation for individual type

Fig. 6 (continued)

flooding of highly porous and permeable reservoirs is more serious (Zhang et al. 2016).

Method application

The method in this paper is applied to an inject-product unit in the study area, which includes six wells, namely one injection well#f and five oil production wells (#a, #b, #c, #d, and #e); the connected sand layers between the water injection wells and the oil production wells in the unit are S22 and S26. The unit has been water flooded, and some oil production wells have produced a certain amount of injected water. Since the layers S22 and S26 in the study area are sand layers with high porosity and permeability, the logging data can be used to establish the effective calculation formula of porosity (ϕ), permeability (k), and shale content (V_{sh}) (Hong 2008; Wang et al. 2019). Equations (16), (17), and (20), respectively, are the calculation formulas of ϕ , V_{sh} , and k in the study area. The water saturation Sw_0 from deep lateral resistivity (LLD) can be calculated by using Archie’s formula (Bussian 1982), see Eq. (21):

$$\phi = -0.001AC^2 + 0.7887AC - 117.48(R^2 = 0.933, RMSE = 1.3519) \tag{16}$$

$$V_{sh} = \frac{2^{2-dgr} - 1}{2^2 - 1} (RMSE = 1.052) \tag{17}$$

$$dgr_1 = (GR - grmin)/(grmax - grmin) \tag{18}$$

$$dgr_2 = 1 - PSP/SSP \tag{19}$$

$$\ln(k) = -27.4096 - 0.0681dgr + 0.1124AC (R^2 = 0.901, \text{Mean Relative Error} = 81.352\%) \tag{20}$$

$$Sw_0 = \sqrt{\frac{R_w}{LLD \cdot \phi^2}} \tag{21}$$

where AC is acoustic log value, $\mu\text{s/m}$. When the rock layer does not contain radioactive elements, and the natural gamma curve does not show abnormal values, dgr is taken as dgr_1 ; otherwise, dgr is taken as the minimum value of dgr_1 and dgr_2 . dgr_1 is the change value of natural gamma measurement value relative to pure shale, decimal. In the formula (18), GR is the natural gamma measurement value, API. $grmax$ is the natural gamma value of pure shale, API. $grmin$ is the natural gamma value of pure sandstone, API. In the formula (19), PSP is the amplitude difference of the spontaneous potential curve deviating from the shale baseline, mV; SSP is the amplitude difference of the natural potential curve of the pure sandstone deviating from the shale baseline in the area, mV. R_w is the formation water resistivity value, which is taken as the measured values of the resistivity of the produced water from the S22 and S26 layers of adjacent oil wells in this paper. The R_w values of S22 and S26 are $0.62 \Omega \text{ m}$ and $0.55 \Omega \text{ m}$, respectively. LLD is the deep lateral resistivity log, $\Omega \text{ m}$.

It is assumed that the influence of water flooding mining on the water saturation, porosity, permeability, and shale content of the rock layer is negligible. Logging is a continuous measurement process, and there are many measurement points in a section of the rock layer, but according to the layering and valuing rule of the logging curve, the logging value representing the sand body layer can be reasonably given out (Zhang et al. 2009). The porosity, permeability, and shale content of S22 and S26 sand layers of six wells were calculated using formulas (16)–(20), see Table 4. Also,

Table 4 Reservoir parameters calculated from logging data and current water cutting rates of S22 and S26 in the injection-production unit

Well	Layer number	Porosity (%)	Permeability k (mD)	Shale content V_{sh} (%)	Water cutting rate f_w (%)
Well#a	S22	31.0	1327.4	8.9	0.15
Well#a	S26	28.5	824.0	10.7	0.3
Well#b	S22	19.2	54.5	18.3	0.25
Well#b	S26	27.2	785.3	9.1	0.35
Well#c	S22	27.5	254.1	9.1	0.1
Well#c	S26	21.2	136.7	15.0	0.2
Well#d	S22	30.9	1050.3	7.3	0.35
Well#d	S26	28.7	788.9	9.9	0.3
Well#e	S22	24.9	321.9	7.6	0.45
Well#e	S26	31.0	1078.1	7.3	0.35
Well#f	S22	29.8	393.3	9.0	1.0
Well#f	S26	29.2	331.5	8.3	1.0

Table 5 The relevant parameters of S22 and S26 layers were calculated from the water cutting rates in the inject-product unit

Well	Layer number	R_c		S_{wi}	S_{or}	S_w	Water saturation rate of change S'_w	Layer's type	
Well#a	S22	6.542	4.324	1.534	0.280	0.249	0.389	0.285	First
Well#a	S26	5.379	3.197	1.585	0.295	0.265	0.381	0.208	Second
Well#b	S22	1.684	1.226	1.748	0.355	0.334	0.378	0.089	Third
Well#b	S26	5.376	3.195	1.586	0.290	0.269	0.387	0.210	First
Well#c	S22	3.040	1.743	1.688	0.321	0.289	0.428	0.183	Second
Well#c	S26	2.540	1.531	1.710	0.359	0.313	0.396	0.121	Third
Well#d	S22	5.827	3.592	1.566	0.257	0.256	0.391	0.249	First
Well#d	S26	5.240	3.084	1.592	0.295	0.265	0.475	0.318	First
Well#e	S22	3.599	2.015	1.664	0.309	0.290	0.410	0.158	Second
Well#e	S26	5.900	3.660	1.562	0.276	0.255	0.421	0.257	First
Well#f	S22	3.634	2.033	1.662	0.309	0.276	0.724		
Well#f	S26	3.368	1.898	1.674	0.311	0.280	0.720		

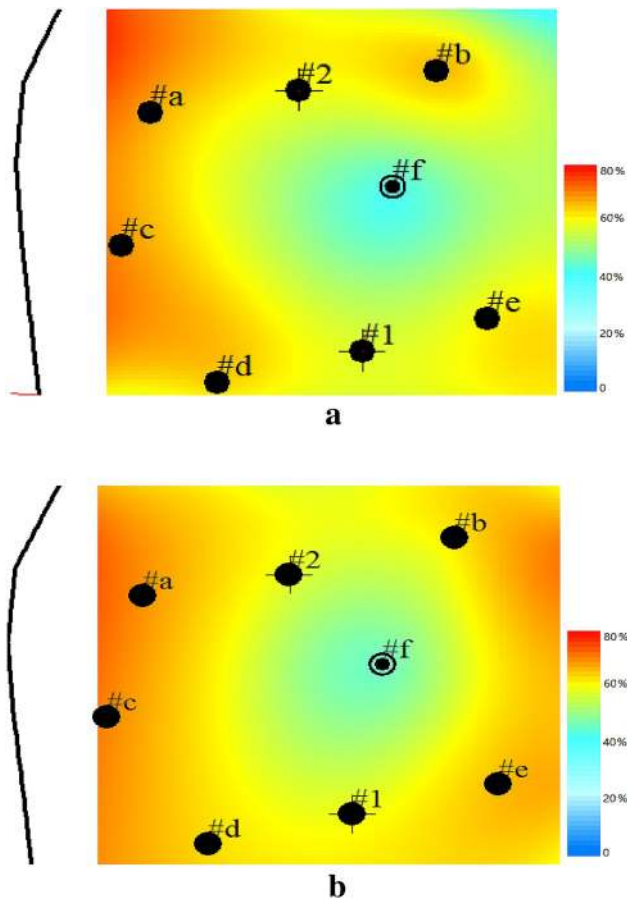


Fig. 7 **a** Distribution of remaining oil saturation of S22 layer in the injection and production unit, **b** distribution of remaining oil saturation of S26 layer in the injection and production unit

Table 4 gives the current water cutting rate of each layer. And the water cutting rate of the water injection well#f was taken as 1.0. The coefficients c and n , bound water saturation S_{wi} , and residual oil saturation S_{or} were calculated by using formulas (11–14), respectively. The water cutting rates of the S22 and S26 layers of each well were, respectively, brought into formula (5) and formula (15) to calculate the water saturation S_w and the change rate of water saturation S'_w . The calculation results are shown in Table 5. The remaining oil saturation of each layer was calculated by formula (6), and the contour map of the remaining oil saturation distribution of the inject-product unit was drawn in the way of interpolation, as shown in Fig. 7a, b. Table 5 shows that the remaining oil saturation S_o of the S22 and S26 layers is about 60%. In Table 5, the type of each rock layer was determined by its R_c and V_{sh} values. According to the analysis of S'_w above, the S'_w values of layers in the first type group all are less than 0.331, and the S'_w values of layers in the second type group all are less than 0.211; the S'_w values of layers in the third type group all are less than 0.125. That means the change rates of water saturation of the S22 and S26 layers of the six production wells are laying in the stable section, the remaining oil distribution is proper, and the sand body is suitable for continuous mining.

Therefore, two infill wells #1 and #2 were deployed. Layered mining for these two wells individually was carried out, the water cutting rate of the two layers S22 and S26 in well#1 reached 95% and 50%, respectively, and the water content of the two layers S22 and S26 in well#2 reached 30% and 40%, respectively. According to the remaining oil saturation distribution results of this unit, it

Table 6 Water cutting rates and reservoir parameters calculated by logs of infill well#1 and well#2

Well	Layer number	Porosity (%)	Permeability k (mD)	Shale content V_{sh} (%)	Water saturation Sw_0 (%)	Water cutting rate f_w (%)
Well#1	S22	29.5	1389.26	8.9	37.1	0.95
Well#1	S26	25.2	917.0	9.9	43.2	0.5
Well#2	S22	26.7	192.4	10.4	36.9	0.3
Well#2	S26	22.4	199.7	9.8	44.6	0.4

Table 7 The relative parameters deduced from water cutting rates of infill well#1 and well#2

Well	Layer number	R_c	S_{wi}	S_{or}	S_w	Water saturation rate of change S'_w		
Well#1	S22	6.862	4.699	1.520	0.234	0.199	0.677	1.356
Well#1	S26	6.032	3.788	1.557	0.252	0.224	0.417	0.294
Well#2	S22	2.683	1.588	1.704	0.333	0.295	0.344	0.133
Well#2	S26	2.984	1.717	1.691	0.329	0.304	0.426	0.141

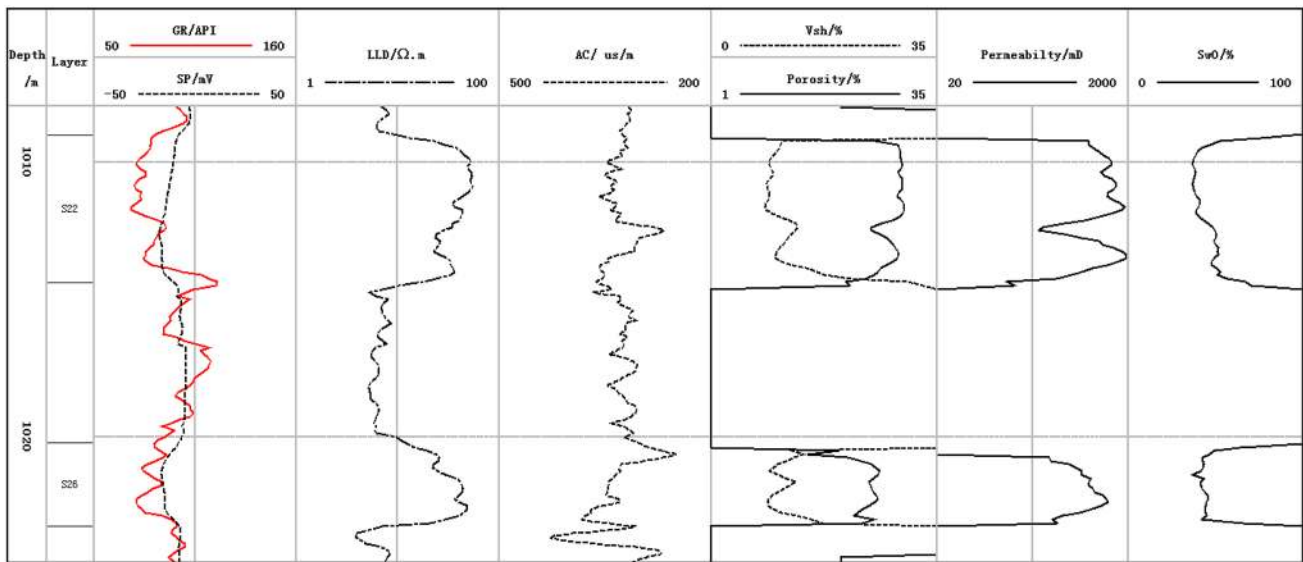


Fig. 8 Logging curves and related parameters calculated by logs of infill well#1. (From the left track to the right track, the first track is well depth, in m; the second track is the layer’s number; the third track is deep dual lateral resistivity log, LLD Ω m; the fourth is

acoustic log, us/m; the fifth track is shale content curve V_{sh} , %, and porosity ϕ , %; the sixth track is permeability k , mD; the last track is the saturation curve from well logs Sw_0 , %)

is unreasonable that the water cutting rate of the S22 layer in well#1 reaches 95%. Table 6 shows the porosity, permeability, and mud content calculated from logging data in wells #1 and #2, as well as the current water cutting rate. The coefficient c and n , bound water saturation S'_{w} , residual oil saturation S_{or} , water saturation S_w , and the change rate of water saturation S'_w were calculated by using the relevant formulas above. Table 7 shows the calculation results. S_w of the S22 and S26 layers of well#1 is 68.4% and 41.7%, respectively, and S'_w is 1.316 and 0.294. S_w of the S22 and S26 layers of well#2 is 34.4% and 42.6%, respectively, and S'_w is 0.133 and 0.141.

According to Eq. (21), the Sw_0 values of S22 and S26 in well#1 are 37.1% and 43.2%, respectively. Sw_0 values of S22 and S26 in wells #2 are 36.9% and 44.6%, respectively. Compared with Table 5, it is found that except for well#1 layer S22, the Sw values of the other three layers are equivalent to Sw_0 , indicating that the water saturation method calculated from the water cutting rate in this paper is reasonable. Figure 8 shows the logging curves of the natural gamma ray (GR), spontaneous potential (SP), deep lateral resistivity (LLD) log, acoustic log (AC), and the porosity (ϕ), permeability (k), shale content (V_{sh}), and water saturation curve (Sw_0) are calculated by logging curves. From Sw_0 curve, in

the bottom part (well section is 1012.5–1014.5 m) S_{w0} is about 55% deviating from 37% in the up part (well section is 1009.2–1012.5 m). And from k curve, k changes from 231 to 1913 mD, and it means S22 layer is severe heterogeneity. It is conceivable that there are macrochannels for injection water to circulate it low efficiently in the high-permeability strip (Chen et al. 2019; Skjaerstein et al. 1997). Under this suggestion, profile control and plugging treatments were carried out on the high-permeability strip of S22, and the water cutting rate lowered down to 39%. It is consistent with the log calculation S_{w0} , and it indicates that this layer is in a period of stable exploitation.

Conclusion

1. The index percolating saturation formula reflects the productive relationship between permeability, water saturation, and water cutting rate. However, it is not the unique relationship; the coefficients in the formula are strictly related to the porosity and permeability characteristics of samples. The relationship between pore structure parameters R_c and index formula's coefficients was established by optimizing core experimental data which have a good fit.
2. The coefficients, bound water saturation, and residual oil saturation in the index saturation formula can be determined by the porosity, permeability, and shale content of a rock layer. These three parameters can be calculated from the logs effectively. The percolating saturation formula with variable coefficients constructed in this way conforms to the actual situation of different rock properties and different exploit effects.
3. The law of rock saturation changing with water yield is given by establishing the derivative relationship between water saturation and water cutting rate. When the water cutting rate is less than 20%, that is, under the condition of low water flooding, the change of water saturation is slower than that of water cutting rate. Under medium water flooding condition (water cutting rate is 20–80%), reservoir water saturation decreases uniformly. Under high water flooding condition (water cutting rate is greater than 80%), the water saturation in the layer changes sharply with the water cutting rate; at this point, the reservoir is almost depleted, and injected water completely replaces the original underground fluid.
4. Although the study did not consider actual conditions such as gravity and capillary forces, it can be used as an ideal background to analyze the dynamic information in actual mining. For instance, the water cutting rate of some oil reservoirs is above 95% at the beginning of exploitation. The reservoir likely has a “macrochannel” for inefficient circulation. It does not mean that the remaining oil saturation in the layers tends to 0.
5. According to the research method of the paper, the remaining oil saturation is predicted for a well block that has been exploited for many years, while the water cutting rate in the production process of the oil layers was combined with the reservoir parameters such as porosity, permeability, and shale content of the rock layer. Because no new drilling is required, it saves a lot of drilling cost and guarantees the improvement in the oil recovery capacity of the oilfield that has been developed for many years. This job has a vital promotion significance.

Acknowledgements This research work was jointly funded by the National Natural Science Foundation of China (41172135) and Natural Science Foundation of Heilongjiang (2020). Thanks are also due to Daqing Oilfield Limited Company for data preparation and permission to publish this paper. We thank the editors and reviewers for their valuable comments on this paper. These comments have greatly improved our paper.

Open Access This article is licensed under a Creative Commons Attribution 4.0 International License, which permits use, sharing, adaptation, distribution and reproduction in any medium or format, as long as you give appropriate credit to the original author(s) and the source, provide a link to the Creative Commons licence, and indicate if changes were made. The images or other third party material in this article are included in the article's Creative Commons licence, unless indicated otherwise in a credit line to the material. If material is not included in the article's Creative Commons licence and your intended use is not permitted by statutory regulation or exceeds the permitted use, you will need to obtain permission directly from the copyright holder. To view a copy of this licence, visit <http://creativecommons.org/licenses/by/4.0/>.

References

- Abrams A (1975) The influence of fluid viscosity, interfacial tension, and flow velocity on residual oil saturation left by waterflood. Soc Pet Eng J 15(05):437–447
- Alfarge D, Wei M, Bai B et al (2017) Numerical simulation study of factors affecting relative permeability modification for water-shutoff treatments. Fuel 207:226–239
- An S, Yao J, Yongfei Y et al (2016) Influence of pore structure parameters on flow characteristics based on a digital rock and the pore network model. J Nat Gas Sci Eng 31:156–163
- Andersen PØ, Standnes DC, Skjæveland SM (2017) Waterflooding oil-saturated core samples—analytical solutions for steady-state capillary end effects and correction of residual saturation. J Pet Sci Eng 157:364–379. <https://doi.org/10.1016/j.petrol.2017.07.027>
- Burdine NT (1953) Relative permeability calculations from pore size distribution data. Pet Trans Am Inst Mining Metall Eng 198(3):71–78
- Bussian AE (1982) A generalized Archie equation. SPWLA 23th annual logging symposium, society of petrophysicists and well-log analysts, Corpus Christi, Texas
- Chen C, Han X, Yang M et al (2019) A new artificial intelligence recognition method of dominant channel based on principal component analysis. In: SPE/IATMI Asia Pacific oil & gas conference and exhibition. Society of Petroleum Engineers

- Cobb WM, Marek FJ (1997) Determination of volumetric sweep efficiency in nature Water flood using production data. In: SPE, 38902
- Crotti MA, Cobenas RH (2001) Scaling up of laboratory relative permeability curves. An. Society of Petroleum Engineers Journal, 2001, Paper (SPE 69394)
- Dullien FAL, Dhawan GK, Gurak N et al (1972) A relationship between pore structure and residual oil saturation in tertiary surfactant floods. Soc Pet Eng J 12(04):289–296. <https://doi.org/10.2118/3040-pa>
- Elkins LF, Poppe RE (1973) Determining residual oil saturation behind a waterflood—a case history. J Pet Technol 25(11):1237–1243. <https://doi.org/10.2118/3788-pa>
- Feng Q, Zhang J, Wang S et al (2017) Unified relative permeability model and water flooding type curves under different levels of water cut. J Pet Sci Eng 154:204–216
- Gong P, Liu B, Zhang J et al (2018) Classification study on relative permeability curves. World J Eng Technol 6(04):723
- Haralick RM, Shanmugam K (2007) Computer classification of reservoir sandstones. IEEE Trans Geosci Electron 11(4):171–177
- Hirasaki GJ (1996) Dependence of waterflood remaining oil saturation on relative permeability, capillary pressure, and reservoir parameters in mixed-wet turbidite sands. SPE Reserv Eng 11(02):87–92. <https://doi.org/10.2118/30763-pa>
- Hong Y (2008) Logging principle and comprehensive interpretation. China University of Petroleum Press, Peking, pp 80–100
- Hou QJ, Feng ZQ, Feng ZH (2009) Continental petroleum geology of Songliao Basin. Petroleum Industry Press, Peking, pp 307–315
- Hu X, Yuanling G, Jie H et al (2005) Physical significance and variation characteristics of water cut and water saturation linear model. Fault-Block Oil Gas Field 12(3):55–57 (In chinese)
- Jones SC, Roszelle WO (1978) Graphical techniques for determining relative permeability from displacement experiments. J Pet Technol 30(05):807–817
- Lala AMS, El-Sayed NAA (2015) Controls of pore throat radius distribution on permeability. Geofluids. <https://doi.org/10.1111/gff.12158>
- Li SX, Chen YM (2001) Using interwell tracer test to determine the remaining oil saturation. Pet Explor Dev 28(2):73–75
- Ma S, Morrow NR (1996) Relationships between porosity and permeability for porous rocks. In: International symposium of the society of core analysts, September, pp 8–10
- Meiling Z, Lili L, Guibin D et al (2009) Stratified evaluation technique for continuous lithologic profile logging in exploration and evaluation wells. J Daqing Pet Inst 33(05):41–46 (In chinese)
- Pittman ED (1992) Relationship of porosity and permeability to various parameters derived from mercury injection-capillary pressure curves for sandstone. AAPG Bull 76(2):191–198. <https://doi.org/10.1306/BDF87A4-1718-11D7-8645000102C1865D>
- Rathmell JJ, Braun PH, Perkins TK (1973) Reservoir waterflood residual oil saturation from laboratory tests. J Pet Technol 25(02):175–185
- Renard G, Dembele D, Lessi J, et al (1998) System identification approach applied to watercut analysis in waterflooded layered reservoirs. In: SPE/DOE improved oil recovery symposium, pp 35–47. <https://doi.org/10.2523/39606-ms>
- Shen P et al (1995) Oil layer physics experiment technology. Petroleum Industry Press, Beijing, pp 21–71. (In chinese)
- Singh H, Myshakin E M, Seol Y (2019) A nonempirical relative permeability model for hydrate-bearing sediments. Soc Pet Eng J, Paper (SPE 193996)
- Skjaerstein A, Tronvoll J, Santarelli FJ et al (1997) Effect of water breakthrough on sand production: experimental and field evidence. In: SPE annual technical conference and exhibition. Society of Petroleum Engineers
- Wang XD, Yang SC, Wang Y (2019) Improved permeability prediction based on the feature engineering of petrophysics and fuzzy logic analysis in low porosity-permeability reservoir. J Pet Explor Prod Technol 9(2):869–887
- Li WQ, Yin TJ, Deng ZH et al (2016) Waterflooding characteristics of sealed coring wells in Beiexi area of Saertu oilfield. Pet Geol Recov Effic 23(1):101–106 (In chinese)
- Welge HJ, Johnson EF, Hicks AL et al (1962) An analysis for predicting the performance of cone-shaped reservoirs receiving gas or water injection. J Pet Technol 14(08):894–898
- Lu XG, Zhao YS et al (1995) Application and evaluation of reservoir classification method. Pet Geol Oil Field Dev Daqing, NO.3, 10–15 (In chinese)
- Xie J, Zhang J et al (2003) Residual oil description and prediction. Petroleum Industry Press, pp 111–121. (In chinese)
- Xie Y, Du Z, Chen Z et al (2017) Simplified pore network model for analysis of flow capacity and residual oil saturation distribution based on computerized tomography. Chem Technol Fuels Oils 53(4):579–591
- Xu F, Mu L, Wu X et al (2014) New expression of oil/water relative permeability ratio vs. water saturation and its application in water flooding curve. Energy Explor Exploit 32(5):817–830
- Yang S (1998) A practical method for obtaining residual oil saturation. J Pet Univ (Nat Sci Edn) 22(2):14–16 In Chinese
- Yu QT (1982) Two types of changes of the rate of water cut with recovery factor and the corresponding relative oil-water permeability curves for water-drive reservoirs. Acta Pet Sin 3(4):29–37
- Zahoor MK (2015) Comparative analysis of relative permeability models with reference to extreme saturation limit and its influence on reservoir performance prediction. Sains Malaysiana 44(10):1407–1415. <https://doi.org/10.17576/jsm-2015-4410-05>
- Zhang S, Zhang M, Ke Z (2013) Researches on the oil-water distribution laws of the reservoirs by complex pore structure parameters. Pet Geol Oilfield Dev Daqing 32(2):127–131 In chinese
- Zhang M, Qi M, Lin L (2016) Comprehensive evaluation method of waterflooded layer in extra-low permeability reservoir of daqing peripheral oilfield, lithologic oil-gas reservoir, 28(2): 93–101. (In chinese)
- Zhang Y, Zhang H et al (2018) The influence law of oil relative permeability on water cut. J Geosci Environ Prot 6(09):223